Available online at www.sciencedirect.com
ScienceDirect
Acta Materialia 54 (2006) 4565–4574
Acta MATERIALIA
www.actamat-journals.com

Deformation banding and shear banding in single crystals

S. Mahesh *

Departments of Mechanical and Aerospace Engineering, Indian Institute of Technology, Kanpur 208016, India

Received 12 May 2006; accepted 20 May 2006
Available online 28 August 2006

Abstract

A theory of rigid-plastic single-crystal deformation based on the hypothesis that the crystal follows a mode of deformation that minimizes the plastic power is developed. In addition to the usual homogeneous slip modes, plastic power minimization in the present theory also extends over inhomogeneous deformation modes in the form of deformation bands or shear bands. Bands are assumed to originate from unstable perturbations of the lattice orientation. The evolution of the banded substructure with continued deformation depends on the mobility of the interband dislocation boundaries. The theory predicts the evolution of substructural morphology and lattice orientation with deformation. These predictions agree quantitatively with experimental observations in initially $(1\,1\,2)/[1\,1\,\bar{1}]$- and $(0\,0\,1)/[1\,1\,0]$-oriented copper single crystals that undergo shear banding and deformation banding, respectively, when subjected to plane strain deformation.

Keywords: Deformation band; Shear band; Texture modeling; Rolling; Copper

1. Introduction

A perfect single crystal is characterized by a uniform lattice orientation. When plastically deformed, a single crystal of a medium stacking fault energy metal such as copper may divide into substantially misoriented domains [1] each of which undergoes deformation different from that imposed on the crystal as a whole. This division may be effected over a wide range of length scales [2,3]. At the coarsest scale the crystal may divide into lath-shaped regions, with a width of several tens of dislocation mean free paths and long enough to extend across the entire crystal. Depending on their morphology, such regions are either termed deformation bands [4–6] or shear bands [7,8]. On a finer scale, the crystal may divide into regions called cell blocks whose dimension is of the order of a few dislocation mean free paths. Cell blocks are demarcated by dislocation structures called dense dislocation walls and/or microbands [9]. On the finest scale, the crystal may be divided by incidental dislocation boundaries that arise from the statistical trapping of glide dislocations, whose average separation is the mean free path of dislocations. The nature of the subdivision (presence or absence of each of the three scales of subdivision, microstructural morphology, lattice misorientation across demarcating boundaries, etc.) is known to depend on the lattice orientation of the initial crystal with respect to the imposed deformation [10].

The present work is concerned primarily with deformation and shear bands in single crystals. Whereas deformation banding refers to crystal division into two or more regions of comparable size that undergo comparable deformation [4–6], shear banding refers to an uneven division wherein the smaller domain undergoes the bulk of the deformation primarily by way of simple shear. Shear banding is always preceded by the formation of obstacles to homogeneous dislocation glide in the crystal. If the precursory obstacles are fine twin lamellae [11–13], shear bands are classified as brass type; if they are dislocation walls of a cell block structure [8], the shear bands are said to be of the copper type.

The theoretical and experimental literature on crystal banding is vast. Below, we summarize three theories of banding. The first of these theories was developed by Hill [14], Rudnicki and Rice [15], Asaro and co-workers [16–18], and Anand and Spitzig [19,20]. It views localized deformation

* Tel.: +91 512 259 6024; fax: +91 512 259 7561.
E-mail address: smahesh@iitk.ac.in.

1359-6454/$30.00
doi:10.1016/j.actamat.2006.05.043

as an instability in the macroscopic constitutive description of the inelastic deformation of the material. Shear bands develop, according to this theory, when the elastoplastic field equations admit an inhomogeneous velocity field as solution. In agreement with experimental observations, this theory exhibits shear banding even in a hardening material [17,18] and correctly predicts the orientation of shear bands [17–20].

The second theory, due to Dillamore et al. [21] and Van Houtte et al. [22] starts with the following criterion of material instability: if $\hat{\sigma}$ denotes a stress measure and $\hat{\varepsilon}$ denotes a plastic strain measure, then the condition for localized deformation is given by $\mathrm{d}\hat{\sigma}/\mathrm{d}\hat{\varepsilon} \leqslant 0$. As in the first approach, these authors have shown that shear banding can be achieved even in a hardening material if one accounts for geometric softening. In Dillamore et al.'s theory, the orientation of the shear band will be that which maximizes geometric softening.

The third theory is due to Lee and co-workers [4,23] and Ortiz and co-workers [24,25]. Based on experimental observations of patchy slip in single crystals (wherein spatially isolated single slipping domains are observed after deformation), it has been conjectured at least since 1935 [26] that deformation in a crystal occurs so as to minimize latent hardening. The variational theory of Ortiz and Repetto [24] develops this conjecture by choosing the mode of crystal deformation (including banding) that minimizes the work of plastic deformation. This criterion causes crystal banding because plastic work can be reduced by lowering latent hardening, which in turn can be reduced if multislip activity in a homogeneously deforming crystal is replaced with single slip activity within spatially isolated bands. Thus, latent hardening of slip systems is necessary for banding in this theory.

The first theory mentioned above [14,15,17–20] is predicated on a macroscopic stability criterion, and the second theory [21,22] is based on plastic power minimization and maximum geometric softening criteria. These theories therefore neither account for nor predict aspects of the microstructural phenomena of banding. The third theory [24,25] does account for the energy stored between bands in the form of geometrically necessary dislocations, and includes it in the plastic work minimized during the overall deformation. However, this theory too leaves the causative physical phenomena of banding unaccounted for, because its variational banding hypothesis (minimizing plastic work over the entire deformation history) links band formation at any instant to deformation after that instant as well, and cannot therefore be regarded as a causative physical phenomenon.

The present theory of crystal banding differs fundamentally from the above theories in that it aims to describe the microstructural phenomena of banding. Our motivation thus most closely parallels that behind the experimental work of Korbel and co-workers [27–29]. Following Mahesh and Tomé [30], we hypothesize that banding is initiated stochastically from small perturbations in lattice orientation. These perturbations lead to small perturbations in the local deformation field, which may unstably increase the lattice perturbation provided (1) the inhomogeneous deformation dissipates less plastic power than the homogeneous deformation, and (2) the crystal is orientationally unstable (defined in Section 2.4) in the favored inhomogeneous deformation mode given by (1). Condition (1) is based on an extension of these well-established Taylor postulate [31] due to Chin and Wonsiewicz [32]. Banding or otherwise at any instant is predicted by the above criterion using only the state of the crystal and the imposed deformation rate at that instant. These determine the instantaneous plastic power of deformation. We also hypothesize that a banded crystal deforms so as to minimize plastic power with continued deformation. Based on conditions (1) and (2) above, the present theory predicts (possibly inhomogeneous) crystal deformation that maximizes geometric softening, and reduces latent hardening, which are fundamental assumptions of the previous theories. Also, the present theory applies to both deformation and shear banding, predicts banded substructure morphology and misorientation evolution, and gives detailed insight into the accompanying substructural transitions.

The plan of this paper is as follows. Section 2 details the present theory. Section 3 introduces the phenomenology needed to represent the substructural state. Section 4 compares the present predictions with experimental results from the literature for two well-studied copper crystals under rolling deformation.

2. Theory of banding

2.1. Constitutive law

The crystal is modeled as a rigid-plastic material deforming according to the viscoplastic constitutive law. If $\dot{\boldsymbol{\varepsilon}}$ denotes the strain rate in a crystal or band whose S slip systems indexed by s have unit normals $\boldsymbol{n}^s$ and unit Burgers vectors $\boldsymbol{b}^s$ the crystal constitutive response is taken to follow [35,36]

$$\dot{\boldsymbol{\varepsilon}} = \sum_{s=1}^{S} \mathbf{m}^s \left| \frac{\boldsymbol{\sigma} : \mathbf{m}^s}{\tau^s} \right|^n \operatorname{sign}(\boldsymbol{\sigma} : \mathbf{m}^s), \tag{1}$$

where $\boldsymbol{\sigma}$ is the Cauchy stress, τ^s is the critical resolved shear stress of slip system s, n is the reciprocal rate sensitivity, and the Schmid tensor $\boldsymbol{m}^s$ of slip system s is given by

$$\mathbf{m}^s = (\mathbf{n}^s \otimes \mathbf{b}^s + \mathbf{b}^s \otimes \mathbf{n}^s)/2; \quad s = 1, \ldots, S. \tag{2}$$

Taking the slip rate $\dot{\gamma}^s$ in slip system s

$$\dot{\gamma}^s = \left| \frac{\boldsymbol{\sigma} : \mathbf{m}^s}{\tau^s} \right|^n \operatorname{sign}(\boldsymbol{\sigma} : \mathbf{m}^s), \tag{3}$$

we may express Eq. (1) in the form $\dot{\boldsymbol{\varepsilon}} = \sum_s \dot{\gamma}^s \mathbf{m}^s$.

2.2. Plastic power of a banded crystal

Consider a crystal divided into two types of (not necessarily contiguous (Fig. 10 of Ref. [23])) domains called

bands with volume fractions $0 \leqslant w^{(1)} \leqslant 1$ and $w^{(2)} = 1 - w^{(1)}$. Let the uniform lattice orientation of the bands be specified by orthonormal tensors $\boldsymbol{g}^{(1)}$ and $\boldsymbol{g}^{(2)}$ that quantify the rotation to be imparted to bring the sample and lattice coordinate systems into coincidence in each band. Let the critical resolved shear stress in slip system s of band i be $\tau^{s,\,(i)}, i = 1,2$. $(\boldsymbol{g}^{(1)}, \boldsymbol{g}^{(2)})$ completely determine the Schmid tensors $\boldsymbol{m}^{s,(1)}$ and $\boldsymbol{m}^{s,(2)}$, $s = 1,\ldots,S$ in the bands. So if the bands are known to deform with strain rates $\dot{\boldsymbol{\varepsilon}}^{(1)}$ and $\dot{\boldsymbol{\varepsilon}}^{(2)}$, and have known critical resolved shear stress $(\tau^{s,(1)}, \tau^{s,(2)})$, their respective Cauchy stresses $\boldsymbol{\sigma}^{(1)}$ and $\boldsymbol{\sigma}^{(2)}$ are determined by Eq. (1). The plastic power of deformation of the banded crystal is defined as

$$\dot{W}^{\mathrm{def}}(w^{(1)}, w^{(2)}, \dot{\boldsymbol{\varepsilon}}^{(1)}, \dot{\boldsymbol{\varepsilon}}^{(2)}, \mathbf{g}^{(1)}, \mathbf{g}^{(2)}) = w^{(1)}\dot{\boldsymbol{\varepsilon}}^{(1)} : \boldsymbol{\sigma}^{(1)} + w^{(2)}\dot{\boldsymbol{\varepsilon}}^{(2)} : \boldsymbol{\sigma}^{(2)}. \tag{4}$$

In discussing banding in the rest of Sections 2.2 and 2.3, we assume that the sth critical resolved shear stress in both bands is equal, i.e., $\tau^{s,(1)} = \tau^{s,(2)}$, for all s. Homogeneous deformation of the crystal corresponds to $\dot{\boldsymbol{\varepsilon}}^{(1)} = \dot{\boldsymbol{\varepsilon}}^{(2)}$, $\boldsymbol{g}^{(1)} = \boldsymbol{g}^{(2)}$, and $\boldsymbol{\sigma}^{(1)} = \boldsymbol{\sigma}^{(2)}$.

Let us first consider a banded crystal with $\boldsymbol{g} = \boldsymbol{g}^{(1)} = \boldsymbol{g}^{(2)}$, whose bands are subjected to strain rates $\dot{\boldsymbol{\varepsilon}}^{(1)}$ and $\dot{\boldsymbol{\varepsilon}}^{(2)}$ that satisfy

$$w^{(1)}\dot{\boldsymbol{\varepsilon}}^{(1)} + w^{(2)}\dot{\boldsymbol{\varepsilon}}^{(2)} = \bar{\dot{\boldsymbol{\varepsilon}}}, \tag{5}$$

where $\bar{\dot{\boldsymbol{\varepsilon}}}$ denotes the overall strain rate imposed on the crystal. The following inequality then follows from the convexity of $\dot{W}^{\mathrm{def}}$ [24]:

$$\dot{W}^{\mathrm{def}}(w^{(1)}, w^{(2)}, \dot{\boldsymbol{\varepsilon}}^{(1)}, \dot{\boldsymbol{\varepsilon}}^{(2)}, \mathbf{g}, \mathbf{g}) \geqslant \dot{W}^{\mathrm{def}}(w^{(1)}, w^{(2)}, \bar{\dot{\boldsymbol{\varepsilon}}}, \bar{\dot{\boldsymbol{\varepsilon}}}, \mathbf{g}, \mathbf{g}) \tag{6}$$

Thus, of all (possibly inhomogeneous) deformations capable of accommodating the deformation imposed on the crystal according to Eq. (5), it is the homogeneous deformation mode that minimizes the plastic power. Eq. (6) effectively precludes satisfaction of the Chin and Wonsiewicz [32] necessary condition for banding. Expressed in terms of deformation rates, this condition requires the power of banded deformation to be smaller than that of homogeneous deformation, i.e.,

$$\dot{W}^{\mathrm{def}}(w^{(1)}, w^{(2)}, \dot{\boldsymbol{\varepsilon}}^{(1)}, \dot{\boldsymbol{\varepsilon}}^{(2)}, \mathbf{g}, \mathbf{g}) + \dot{W}^{\mathrm{acc}} \leqslant \dot{W}^{\mathrm{def}}(w^{(1)}, w^{(2)}, \bar{\dot{\boldsymbol{\varepsilon}}}, \bar{\dot{\boldsymbol{\varepsilon}}}, \mathbf{g}, \mathbf{g}), \tag{7}$$

where the power $\dot{W}^{\mathrm{acc}} \geqslant 0$ is associated with accommodation of incompatibility between the bands and between the crystal and its surroundings.

2.3. Lattice orientation perturbation

Crystals, however, do exhibit small variations in lattice orientation. Even in an initially perfect crystal, these lattice orientation perturbations are caused by incidental dislocation boundaries (IDBs) generated during plastic deformation. Hughes et al. [37] have observed that the misorientation vector across IDBs is uniformly distributed over the unit sphere, that the average misorientation angle $\langle\omega\rangle$ scales with von Mises strain $\varepsilon_{\mathrm{vM}}$ as

$$\langle\omega\rangle = \langle k\rangle\sqrt{\varepsilon_{\mathrm{vM}}}, \tag{8}$$

and that the maximum misorientation angle is $r = 3$–5 times $\langle\omega\rangle$. They find $\langle k\rangle \approx 1^\circ$ for aluminum. The small lattice orientation perturbation induced by IDBs suffices to break the convexity of $\dot{W}^{\mathrm{def}}$ in Eq. (6). For an imperfect crystal ($\boldsymbol{g}^{(1)} \neq \boldsymbol{g}^{(2)}$) the Chin–Wonsiewicz condition suggests the following non-degenerate minimization problem to determine the deformation state:

$$\dot{W}^{\mathrm{def}}_{*} = \min_{C_*} \dot{W}^{\mathrm{def}}(w^{(1)}, w^{(2)}, \dot{\boldsymbol{\varepsilon}}^{(1)}, \dot{\boldsymbol{\varepsilon}}^{(2)}, \mathbf{g}^{(1)}, \mathbf{g}^{(2)}), \tag{9}$$

where minimization is subject to the constraints C_* that (i) $0 \leqslant w^{(1)} \leqslant 1$, $w^{(1)} + w^{(2)} = 1$, (ii) Eq. (5) holds, (iii) if $\boldsymbol{g}$ denotes the average lattice rotation tensor of the crystal, $[\boldsymbol{g}^{(1)}]^{-1}\boldsymbol{g}$ and $[\boldsymbol{g}^{(2)}]^{-1}\boldsymbol{g}$ correspond to a rotation of $-\omega w^{(2)}$ and $\omega w^{(1)}$ about some unit misorientation vector $\hat{\mathbf{m}}$, respectively, (iv) $0 \leqslant \omega \leqslant r\langle\omega\rangle$, and (v)

$$[\dot{\boldsymbol{\varepsilon}}] = \dot{\boldsymbol{\varepsilon}}^{(2)} - \dot{\boldsymbol{\varepsilon}}^{(1)} = (\boldsymbol{\lambda}\otimes\boldsymbol{\nu} + \boldsymbol{\nu}\otimes\boldsymbol{\lambda})/2 \tag{10}$$

for some $\boldsymbol{\lambda}$ and $\boldsymbol{\nu}$. Eq. (10) is necessary to ensure deformation compatibility across the interface between bands with normal $\boldsymbol{\nu}$ [38]. Eq. (10) implies that $\boldsymbol{\lambda} = 2[\dot{\boldsymbol{\varepsilon}}]\boldsymbol{\nu} - ([\dot{\boldsymbol{\varepsilon}}]\boldsymbol{\nu}\cdot\boldsymbol{\nu})\boldsymbol{\nu}$.

The minimization problem in Eq. (9) is readily solved using a projected BFGS scheme [39]. Its solution yields the energetically most favorable configuration of bands. We will refer to this configuration as the nascent banded crystal. The Chin–Wonsiewicz condition takes the form

$$\dot{W}^{\mathrm{def}}(w^{(1)}, w^{(2)}, \dot{\boldsymbol{\varepsilon}}^{(1)}, \dot{\boldsymbol{\varepsilon}}^{(2)}, \mathbf{g}^{(1)}, \mathbf{g}^{(2)}) + \dot{W}^{\mathrm{acc}} \leqslant \dot{W}^{\mathrm{def}}(w^{(1)}, w^{(2)}, \bar{\dot{\boldsymbol{\varepsilon}}}, \bar{\dot{\boldsymbol{\varepsilon}}}, \mathbf{g}, \mathbf{g}) \tag{11}$$

for a nascent banded crystal, subject to Eq. (5), and is typically satisfied because $\dot{W}^{\mathrm{acc}}$ is usually one or two orders of magnitude smaller than the difference between the plastic power terms [40,30] in Eq. (11). This observation, taken together with the experimental observation that not all crystal orientations band, suggests that the banding condition expressed by Eq. (11) is necessary, but overly permissive.

2.4. Lattice orientational stability

If $\boldsymbol{L}^{(1)}$ and $\boldsymbol{L}^{(2)}$ are the velocity gradients in the bands of a nascent banded crystal, compatibility across their common interface requires that [38]

$$[\boldsymbol{L}] = \boldsymbol{L}^{(2)} - \boldsymbol{L}^{(1)} = \boldsymbol{\lambda}\otimes\boldsymbol{\nu}. \tag{12}$$

Eq. (10) assures us of the satisfaction of the symmetric part of this equation. To obtain the rigid spins of the bands needed for compatibility, we decompose $\boldsymbol{L}^{(i)}$, $i = 1,\ 2$ as $\mathbf{L}^{(i)} = \mathbf{L}^{(i)}_{ss} + \mathbf{W}^{(i)}$ where

$$\mathbf{L}^{(i)}_{ss} = \sum_{s=1}^{S} \dot{\gamma}^{s,(i)}\mathbf{b}^{s,(i)}\otimes\mathbf{n}^{s,(i)}, \quad i = 1,\ 2 \tag{13}$$

denotes the velocity gradient associated only with slip activity $\dot{\gamma}^{s,(i)}$ in each band entailing no lattice spin, and the remainder

$$\boldsymbol{W}^{(i)} = \boldsymbol{L}^{(i)} - \boldsymbol{L}^{(i)}_{ss}, \quad i = 1,\ 2 \tag{14}$$

denotes the lattice spin in each band needed to ensure compatibility according to Eq. (12). Substituting Eq. (14) in Eq. (12) we obtain

$$(\mathbf{L}^{(2)}_{ss} + \mathbf{W}^{(2)}) - (\mathbf{L}^{(1)}_{ss} + \mathbf{W}^{(1)}) = \boldsymbol{\lambda} \otimes \boldsymbol{\nu}. \tag{15}$$

Additionally demanding that the average velocity gradient in the crystal equal the imposed velocity gradient, $\overline{\mathbf{L}}$, we have

$$w^{(1)}(\mathbf{L}^{(1)}_{ss} + \mathbf{W}^{(1)}) + w^{(2)}(\mathbf{L}^{(2)}_{ss} + \mathbf{W}^{(2)}) = \overline{\mathbf{L}}. \tag{16}$$

Eqs. (15) and (16) yield

$$\begin{aligned} \mathbf{W}^{(1)} &= \operatorname{skew}\{(\overline{\mathbf{L}} - \langle \mathbf{L}_{ss} \rangle) - w^{(2)}(\boldsymbol{\lambda} \otimes \boldsymbol{\nu} - [\mathbf{L}_{ss}])\} \\ \mathbf{W}^{(2)} &= \operatorname{skew}\{(\overline{\mathbf{L}} - \langle \mathbf{L}_{ss} \rangle) + w^{(1)}(\boldsymbol{\lambda} \otimes \boldsymbol{\nu} - [\mathbf{L}_{ss}])\} \end{aligned} \tag{17}$$

for the lattice spins in the bands, where $\langle \mathbf{L}_{ss} \rangle = w^{(1)}\mathbf{L}^{(1)}_{ss} + w^{(2)}\mathbf{L}^{(2)}_{ss}$ and $[\mathbf{L}_{ss}] = \mathbf{L}^{(2)}_{ss} - \mathbf{L}^{(1)}_{ss}$.

After the imposition of the lattice orientation perturbation, the misorientation between the nascent bands is ω about the optimal unit misorientation vector $\hat{\mathbf{m}}$ (Section 2.3). Further deformation of the crystal may increase or decrease the misorientation between the bands. We term a nascent banded crystal orientationally unstable if the lattice spin of the nascent bands during further deformation increases their misorientation. Otherwise, we term that crystal orientationally stable. Operationally, orientational instability corresponds to $\hat{\mathbf{m}} \cdot [\boldsymbol{w}] > 0$, and orientational stability corresponds to $\hat{\mathbf{m}} \cdot [\boldsymbol{w}] \leqslant 0$, where $[\boldsymbol{w}]$ is the dual vector of the skew tensor $[\boldsymbol{W}] = \boldsymbol{W}^{(2)} - \boldsymbol{W}^{(1)}$ that denotes the relative lattice spin of the nascent bands. We regard orientational instability as a necessary condition for banding to supplement the Chin–Wonsiewicz condition. We will find in Section 4 that orientational instability proves to be the far more stringent condition for banding.

We note here that the present notion of orientational stability fundamentally differs from that of Raabe et al. [41]. Whereas our definition hinges on compatibility across the interband interface of an inhomogeneously deforming nascent banded crystal, Raabe et al.'s definition pertains to a homogeneously deforming lattice orientation perturbed crystal. Compatibility across any interband boundary is automatic in their idealized crystal, and plays no role in determining orientational stability.

2.5. Deformation of a banded crystal

We consider two routes for the evolution of the banded substructure. We term the bands mobile relative to the material if material points may move across the interband boundary during deformation. Thus, band mobility is equivalent to the mobility of the dislocations constituting the interband boundary. Bands that are not mobile will be called immobile.

Let us first consider an immobile band that disallows material exchange with the adjacent band, and whose shape therefore must evolve with the shape of the crystal. The shape of the crystal is described by its deformation gradient, $\boldsymbol{F}$. If $\boldsymbol{\nu}_\mathrm{b}$ denotes the normal to the interband boundary at the instant of banding, corresponding to the crystal deformation gradient $\boldsymbol{F}_\mathrm{b}$, the orientation of the immobile band normal $\boldsymbol{\nu}$ when the deformation gradient of the crystal is $\boldsymbol{F}$ is given as [30]

$$\boldsymbol{\nu} = \mathbf{F}^T_\mathrm{b}\mathbf{F}^{-T}\boldsymbol{\nu}_\mathrm{b} / \left\| \mathbf{F}^T_\mathrm{b}\mathbf{F}^{-T}\boldsymbol{\nu}_\mathrm{b} \right\|. \tag{18}$$

Next, in the case of a mobile band we take the boundary to be oriented so as to minimize $\dot{W}^{\mathrm{def}}$. The solution of the minimization problem

$$\dot{W}^{\mathrm{def}}_{**} = \min_{C_{**}} \dot{W}^{\mathrm{def}}(w^{(1)}, w^{(2)}, \dot{\boldsymbol{\varepsilon}}^{(1)}, \dot{\boldsymbol{\varepsilon}}^{(2)}, \mathbf{g}^{(1)}, \mathbf{g}^{(2)}) \tag{19}$$

then yields the orientation of the normal to the interband boundary, $\boldsymbol{\nu}$. In solving Eq. (19), the lattice orientations, $\boldsymbol{g}^{(1)}$ and $\boldsymbol{g}^{(2)}$, and band volume fractions $w^{(1)}$ and $w^{(2)}$ are held fixed. The minimization is subject to the constraints C_{**} that (i) Eq. (5) and (ii) Eq. (10) hold.

We have described the evolution of $\boldsymbol{\nu}$ with continued deformation of a banded crystal. Compatible deformation across an interband boundary with normal $\boldsymbol{\nu}$ also demands rigid rotation of each band according to Eq. (17). Thus the misorientation across the interband boundary will generally vary with continued deformation.

3. Hardening model and phenomenology

The hardening model for copper used in this work is an extension of the model of Cuitiño and Ortiz [42]. It incorporates the experimental observation of Franciosi and coworkers [43,44] that latent hardening of slip systems is anisotropic and depends on the type of interaction (coplanar interaction, junction formation, etc.) between dislocations in the active and latent slip systems. The interaction between different slip systems is described by a 12×12 square matrix $[A_{st}]$. If ρ_t is the dislocation density in slip system t, the obstacle density in slip system s is taken to be $\sum_t A_{st}\rho_t$.

In the model of Cuitiño and Ortiz, the obstacle density is assumed to be homogeneously distributed throughout the crystal. However, numerous transmission electron microscopy studies (e.g., Refs. [9,10,45]) have revealed that depending on the crystal orientation, the obstacles may be organized in the form of parallel dislocation walls. It is expected that τ^s in the presence of dislocation walls will significantly differ from that in the state of homogeneous obstacle distribution. To account for this, we must identify the crystal orientations that form dislocation walls.

3.1. Condition for dislocation wall formation

In copper undergoing $\langle 1\ 1\ 0 \rangle (1\ 1\ 1)$ slip, let s and s' be a pair of cross-slip systems ($\boldsymbol{b}^s = \boldsymbol{b}^{s'}$) with slip rates $\dot{\gamma}^s$ and $\dot{\gamma}^{s'}$. s and s' are said to be simultaneously activated if

$$1/c_1 \geqslant \left| \dot{\gamma}^s / \dot{\gamma}^{s'} \right| \geqslant c_1, \tag{20}$$

where $0 < c_1 \leqslant 1$ is a fitting parameter. Let $\mathscr{S}$ be the set of all simultaneously activated cross-slip systems and let the slip activity on the crystallographic plane p with normal $\boldsymbol{n}^p$ be

$$\dot{\Gamma}_p = \sum_{s:s\notin\mathscr{S},\mathbf{n}^s=\pm\mathbf{n}^p} |\dot{\gamma}^s|. \tag{21}$$

If p^* and p^{**} are the slip planes with the largest and second largest $\dot{\Gamma}_p$, and

$$\dot{\Gamma}_{p^*}/\dot{\Gamma}_{p^{**}} \geqslant c_2 > 1, \tag{22}$$

we assume that a dislocation wall forms parallel to p^* according to the mechanism suggested by Jackson [46], wherein primary dislocations react with secondary dislocations emitted in the cross-slip system to plastically relax the stress field of the primary dislocations. Slip systems $s \in \mathscr{S}$ are not in accord with this mechanism and are therefore excluded from the computation of $\dot{\Gamma}_p$.

To validate the above phenomenological assumption, Table 1 lists the computed $\dot{\Gamma}_{p^*}/\dot{\Gamma}_{p^{**}}$ under uniaxial tension in eight copper single crystals studied experimentally by Kawasaki and co-workers [47–49] assuming $\tau^1 = \tau^2 = \cdots = \tau^{12}$ and assuming two different sets of boundary conditions representing uniaxial tension along the 1-direction: full constraints (FC) that imposes $\dot{\varepsilon}_{11} = 1$, $\dot{\varepsilon}_{22} = \dot{\varepsilon}_{33} = -0.5$, and $\dot{\varepsilon}_{12} = \dot{\varepsilon}_{13} = \dot{\varepsilon}_{23} = 0$; and relaxed constraints (RC) that imposes $\dot{\varepsilon}_{11} = 1$, $\sigma_{22} = \sigma_{33} = 0$, and $\sigma_{12} = \sigma_{13} = \sigma_{23} = 0$. The experimentally observed substructure in each of the eight crystal orientations has been classified in column 3 following Huang [45]. Type 1 refers to substructures comprising of a single crystallographic dislocation wall, type 2 to substructures with no walls, and type 3 to substructures wherein two non-crystallographic walls were observed. Table 1 suggests that crystals with $\dot{\Gamma}_{p^*}/\dot{\Gamma}_{p^{**}} \gg 1$ form type 1 substructures. If $\dot{\Gamma}_{p^*}/\dot{\Gamma}_{p^{**}} \approx 1$, either type 2 or type 3 substructures form.

We account for the effect of dislocation walls on τ^s only in type 1 crystals since it is in them that the anisotropic hardness correction for the dislocation walls will be largest. In type 1 crystals, we modify Franciosi's interaction matrix $[A_{st}]$ as follows. Let s^* be a slip system in the plane p^*. We scale all A_{ss*} by a factor $b_1 \geqslant 1$, and all A_{s^*t} by a factor $0 < b_2 \leqslant 1$. $b_1 \geqslant 1$ reflects the expectation that dislocations arranged in a continuous wall can, from topological considerations, better obstruct dislocation activity in other slip systems intersecting the wall than when scattered homogeneously throughout the crystal. On the other hand, $0 < b_2 \leqslant 1$ reflects the expectation that dislocations in the wall may be less likely to react with dislocations from other slip systems due to shielding by other dislocations in the wall.

Table 1
Correlation between the experimentally observed substructure after uniaxial tension, and the calculated $\dot{\Gamma}_{p^*}/\dot{\Gamma}_{p^{**}}$ ratio in Eq. (22) obtained from FC and RC calculations (see text)

Tensile axis	Reference	Experimental substructure	$\dot{\Gamma}_{p^*}/\dot{\Gamma}_{p^{**}}$	
			FC	RC
[4 4 1]	[47]	Type 1	2.96	179
[2 2 1]	[47]	Type 1	2×10^4	1.3×10^5
[4 1 5]	[48]	Type 1	2.22	39
[0 0 1]	[49]	Type 2	0/0	0/0
[4 3 3]	[47]	Type 3	1	1
[3 2 2]	[47]	Type 3	1	1
[2 1 1]	[47]	Type 3	1	1
[1 1 1]	[49]	Type 3	0/0	0/0

3.2. Thin domains

A thin domain (e.g., a shear band) is one with at least one dimension comparable to the mean free path of dislocations. Plastic flow in thin domains may be substantially influenced by the boundaries. Here we assume such domains harden isotropically, i.e., $A_{st} = a^{\text{iso}}$, for all s, t.

3.3. Dislocation walls as precursors to shear banding

We assume that type 1 crystals cannot deformation band while type 2 or 3 crystals cannot shear band. This assumption is supported by numerous experimental studies [3,5,8,11,12,27–29,33] wherein obstacles to homogeneous dislocation motion (dislocation walls or fine twin boundaries) have been observed before shear banding, but not before deformation banding. It reflects the physical consideration that shear bands nucleate when piled-up dislocations cut through a pre-existing obstacle structure [50], whereas deformation bands nucleate relatively unhindered by obstacles. Thus, deformation banding appears to be the energetically preferred mode of banding and shear banding a mode that is resorted to only if deformation banding is suppressed by a pre-existing obstacle substructure.

It follows that whereas the volume fractions of the nucleated deformation bands are determined by Eq. (9), those of nucleated shear bands may be determined by the pre-existing obstacle structure. Lacking quantitative information on the precise influence of the precursory obstacles on the nucleated shear band volume we fix $w^{\text{SB}} = f_{\text{SB}}$ at shear band nucleation, where f_{SB} is a parameter, and suppress minimization in Eq. (9) over band volume fractions in type 1 crystals.

3.4. Volume fraction of bands

We assume that only the volume fraction of mobile bands (Section 2.5) can evolve during deformation; the volume fraction of immobile bands is fixed at the instant of banding. Since the crystal itself constitutes a closed system, band volume fractions evolve by material transfer from one band to the other. In order that this occur we deem it necessary that the band l losing material be orientationally unstable (Section 2.4) under the imposed velocity gradient $\boldsymbol{L}^{(l)}$. If this condition is satisfied, we take the evolution rate of the band volume fraction to follow

$$\dot{w}^{(l)} = -\kappa \frac{\partial \dot{W}^{\mathrm{def}}}{\partial w^{(l)}}, \tag{23}$$

where $\dot{w}^{(l)} \leqslant 0$, $l = 1$ or 2, and κ is a fitting parameter.

4. Comparison with experiments

We now calculate the substructural evolution of crystals according to Section 2 using the hardening model and phenomenological assumptions of Section 3 and compare against experimental observations of crystals subjected to rolling or to channel die compression. Throughout, the sample coordinate system coincides with the orthogonal system defined by the rolling (or extrusion), transverse, and normal directions (RD–TD–ND). In this coordinate system, we model both rolling and channel die compression as plane strain deformation with velocity gradient.

$$[\bar{\mathbf{L}}]_{\mathrm{RD-TD-ND}} = \begin{pmatrix} 1 & 0 & 0 \\ 0 & 0 & 0 \\ 0 & 0 & -1 \end{pmatrix}. \tag{24}$$

In all calculations only the $\langle 1\,1\,0\rangle(1\,1\,1)$ slip mode is considered. Schmid–Boas notation [24] is used to identify individual slip systems.

For the purposes of calculation, the imposed deformation is divided into multiple steps, each involving a von Mises strain $\varepsilon_{\mathrm{vM}}$ increment of $0.001\sqrt{4/3}$. Until the crystal bands, with the lattice orientation perturbation determined as in Section 2.3 in each step, the minimization problem Eq. (9) is solved. It is checked if the Chin–Wonsiewicz banding condition (Section 2.3) is satisfied, and if the lattice is orientationally unstable (Section 2.4). If both these tests pass, the crystal is banded, and further computational deformation follows the procedure in Section 2.5. Slip system hardness and lattice orientation of the crystal or of its bands are updated at each step. The parameters used in the present calculations are listed in Table 2.

4.1. Shear banding in a (1 1 2)/[$\bar{1}$ 1 1] crystal

An experimentally well-studied copper crystal orientation that shows shear banding under plane strain deformation is the C-orientation ((ND)/[RD] = (1 1 2)/[$\bar{1}$ 1 1]; Bunge coordinates $(\phi_1, \phi, \phi_2) = (90, 35.26, 45)°$; see Fig. 1). Its microstructural and substructural evolution has been studied by Wagner et al. [8] during rolling and by Jasienski et al. [33] during channel die compression. Both works report initial orientation evolution in the crystal toward the D-orientation ((ND)/[RD] = (4 4 11)/ [$\overline{11}$ $\overline{11}$ 8]; Bunge coordinates (90, 27.21, 45)°). After some strain, shear bands form, followed by reversion of the matrix orientation back toward C, and rapid evolution of shear band orientation toward the C′-orientation ((ND)/[RD] = (1 1 2)/[1 1 $\bar{1}$]; Bunge (90, −35.26, 45)°), and beyond. They also find that the shear bands make angles of 35–50° with the rolling plane.

The orientation of the simulated crystal relative to the sample coordinate axes is shown in Fig. 1. This figure also shows the spherical coordinates $(\theta_{\boldsymbol{\nu}}, \phi_{\boldsymbol{\nu}})$ used to describe the orientation of the normal vector $\boldsymbol{\nu}$ to the interband boundary. During plane strain deformation, the crystal is symmetrically oriented so that pairs of slip systems such as (B2, B4) and (A6, D6) show identical absolute slip rates ($|\dot{\gamma}^{\mathrm{B2}}| = |\dot{\gamma}^{\mathrm{B4}}|, |\dot{\gamma}^{\mathrm{A6}}| = |\dot{\gamma}^{\mathrm{D6}}|$, etc). A standard Taylor calculation with hardening, but without banding, reveals that two coplanar slip systems (CP: B2, B4) and two codirectional slip systems (CD: A6, D6) are activated. In Eq. (22), the B plane represents p^*, and because A6 and D6 are cross-slip activated and all other planes have zero slip rates, $\dot{\Gamma}_{p^{**}} = 0$. Thus, $\dot{\Gamma}_{p^*}/\dot{\Gamma}_{p^{**}} = \infty$ so that a dislocation wall parallel to the B plane must form (Section 3.1) in agreement with experimental observation [8]. Also, according to Section 3.3 this crystal cannot deformation band. We assume that the shear band is a thin domain (Section 3.2) and the matrix is not.

During the initial steps of the calculation, the computer crystal satisfies the Chin–Wonsiewicz necessary banding condition (Eq. (11)) but remains orientationally stable (Section 2.4) until a rolling reduction of 9.5% ($\varepsilon_{\mathrm{vM}} \approx 0.11$). At this point the crystal's lattice orientation is (90, 33.08, 45)° and $\dot{W}^{\mathrm{def}}$ achieves equal minima at two $(\theta_{\boldsymbol{\nu}}, \phi_{\boldsymbol{\nu}})$: (66.9, 0)° and (156.9, 0)°. The first is orientationally stable, while the second is not and therefore represents a computational shear banded state. The calculated shear band forms inclined at $\chi_{\boldsymbol{\nu}} = 180° - \theta_{\boldsymbol{\nu}} = 23.1°$ to the rolling plane (Fig. 1). The optimum misorientation $\hat{\mathbf{m}}$ is parallel to TD, in agreement with Refs. [8,33].

Table 2
Parameters used in the present calculation

Parameter	Reference	Value
n	Eq. (1)	20
c_1	Eq. (20)	0.7
c_2	Eq. (22)	1.2
κ	Eq. (23)	0.005
$r\langle k\rangle$	Section 2.3	3°
b_1	Section 3.1	2
b_2	Section 3.1	0.4
a^{iso}	Section 3.2	3×10^{-3}
f_{SB}	Section 3.3	5%

The hardening parameters for Cu in the Cuitiño–Ortiz [42] model are used without modification and are not reproduced here.

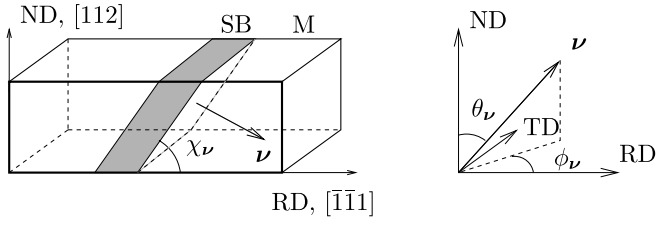

Fig. 1. Initial orientation of the C-oriented crystal relative to the rolling axes. M denotes the matrix and SB the shear band. The spherical coordinates $(\theta_{\boldsymbol{\nu}}, \phi_{\boldsymbol{\nu}})$ specifying the orientation of the normal $\boldsymbol{\nu}$ to the interband boundary are also shown.

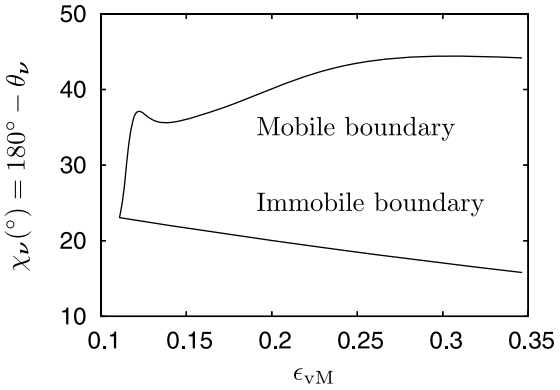

Fig. 2. Evolution of χ_v, the inclination of the shear band to the rolling plane with continued deformation of the banded single crystal.

It is a priori unknown if the shear band is mobile or immobile (Section 2.5). Assuming band mobility, we see from Fig. 2 that χ_v increases with deformation reaching $\chi_v \approx 44.4^\circ$ after 27% rolling reduction. The increase agrees with the experimental observation of Jasienski et al. [33], who also found χ_v distributed between 35° and 50°. The assumption of band immobility, however, rotates the shear band toward alignment with the rolling plane. We therefore conclude that the shear band in the present crystal must be mobile.

With further deformation only the middle Bunge coordinates of the matrix and shear band, ϕ^M and ϕ^{SB}, respectively, evolve as shown in Fig. 3. It is noted that our predictions are in excellent agreement with the measurements of Jasienski et al. [33]: After 27% rolling reduction, the predicted $\phi^M = 34.4^\circ$ agrees well with the measured matrix orientation distribution centered at 34°, and the predicted $\phi^{\mathrm{SB}} = 16.7^\circ$ agrees with the measured shear band orientation distributed between 19.5° and 13.3°.

Fig. 4 shows the calculated evolution of the absolute slip rates $|\dot\gamma|$ in the coplanar (CP: B2 and B4) and codirectional (CD: A6 and D6) slip systems. Before banding, $|\dot\gamma^{\mathrm{CP}}|$ gradually increases and $|\dot\gamma^{\mathrm{CD}}|$ decreases. A dramatic transient slip response develops in the shear band immediately after banding ($0.11 \leqslant \varepsilon_{\mathrm{vM}} \leqslant 0.15$). We believe this to be a calculational artifact induced by the instantaneous transformation of the homogeneous computer crystal into a banded crystal, and expect a softer transient response in the physical crystal accompanying a non-instantaneous shear banding transformation. Outside the transient regime ($\varepsilon_{\mathrm{vM}} \geqslant 0.15$) it is seen that banding has reduced slip activity in the matrix below that in the monolithic crystal. For $\varepsilon_{\mathrm{vM}} \geqslant 0.25$ the CP activity in the shear band dominates all others. In agreement with the experimental observation [8,33] that the shear band deforms much more than the matrix, we find that the computational shear band has accumulated about five times the von Mises strain as the matrix after 27% rolling reduction.

Insight into the nature of the deformation in the shear band at 27% rolling reduction is obtained by examining the velocity gradient $\boldsymbol{L}^{\mathrm{SB}}$ in it, in a coordinate system

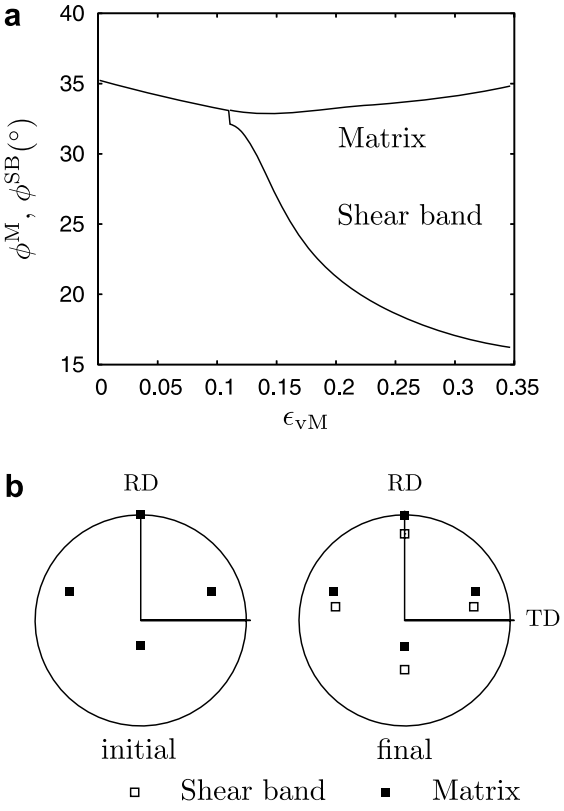

Fig. 3. (a) Evolution with deformation of the middle Bunge angle in the matrix (ϕ^M) and in the shear band (ϕ^{SB}) in an initially C-oriented single crystal. (b) Calculated (1 1 1) pole figures before and after 30% rolling reduction. The pole figures are oriented as in Fig. 3 of Ref. [33] for easy comparison.

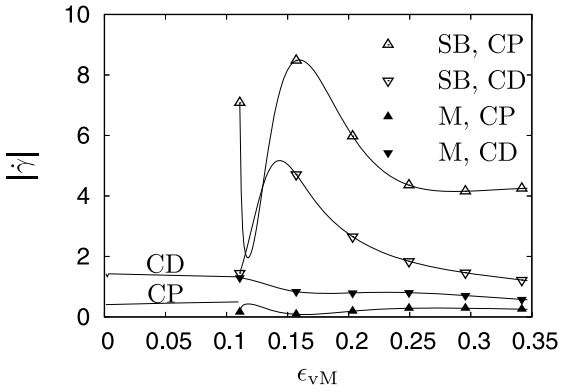

Fig. 4. Evolution of the slip activity in the coplanar (CP) and codirectional (CD) slip systems with von Mises strain in an initially C-oriented Cu crystal.

aligned with the band (obtained by rotating RD–TD–ND through $\chi_v = -44.4^\circ$ about TD):

$$[\mathbf{L}^{\mathrm{SB}}]_{\mathrm{band}} = \begin{pmatrix} 0.02 & 0.00 & -7.10 \\ 0.00 & 0.00 & 0.00 \\ -0.99 & 0.00 & -0.02 \end{pmatrix} \tag{25}$$

The large L^{SB}_{13} indicates that the shear band deforms predominantly under simple shear parallel to the interband boundary. Note that unlike in Refs. [15,17] we have not

presupposed simple shear as the deformation mode of the shear band; approximate simple shear emerges in the present calculation as the minimizer of $\dot{W}^{\text{def}}$ in the banded crystal (Section 2.5).

We next turn to the observation that unlike its copper counterpart, an initially C-oriented aluminum crystal subjected to rolling does not shear band [51,52]. To understand this, we systematically examine the orientational stability of three lattice perturbed ($\omega = 1°$ about TD) crystals oriented between the C and D orientations with $\phi = 33°$, 31°, and 29°. Fig. 5 shows the variation of the orientational stability with hardening anisotropy $\aleph = \tau^{\text{CD}}/\tau^{\text{CP}}$, assuming infinite critical resolved shear stress for the eight slip systems that are neither CP nor CD. It is seen that in all three cases, a critical $\aleph \approx 3.2$ is required to induce orientational instability and banding. We believe this critical hardening anisotropy is never achieved in Al because of its smaller latent hardening ratio than Cu [53]. Franciosi [54] has suggested that the higher stacking fault energy of Al relative to Cu leads to the lower hardening anisotropy of Al because dissociated dislocations, being narrower in Al than in Cu, recombine more readily before passing through an obstacle.

As experimentally evidenced by the observation that the shear bands are uniformly distributed in Wagner et al.'s [8] rolled single crystal but are clustered in a small part of the crystal in Jasienski et al.'s [33] channel die compressed specimen, both of which are nominally plane strain deformed, the width and spacing of shear bands are sensitive to the constraints imposed upon the crystal. We believe that shear band width and spacing are determined by the minimizer of $\dot{W}^{\text{acc}}$ [30]. Accounting for this will turn the present local theory into a non-local one, and we leave this extension to future work.

4.2. Deformation banding in a (0 0 1)/[1 1 0] crystal

Heye and Sattler [34] observed deformation banding in an initially (ND)/[RD] = (0 0 1)/[1 1 0] (Bunge coordinates (−45, 0, 0)°) copper crystal rolled to 75% reduction. They found that the crystal divided into two approximately equal bands with the interband boundary aligned with the rolling plane. With further deformation they found that the bands rotate toward the C and C′ orientations.

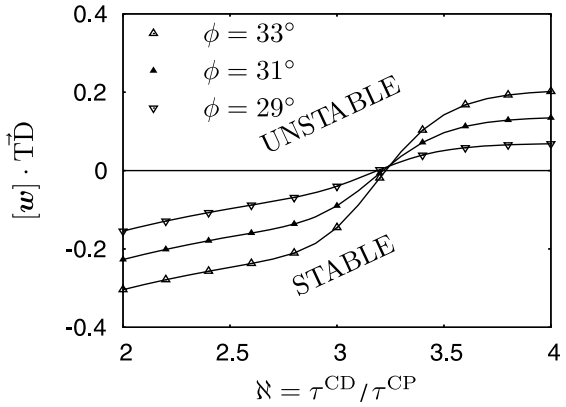

Fig. 5. Dependence of the orientational stability on banding anisotropy $\aleph$ for three crystal orientations between C and D, when the crystal is subjected to plane strain deformation.

A standard Taylor calculation with hardening, but without banding, reveals that two pairs of coplanar slip systems (CP1: C1 and C3; and CP2: B2 and B4) are activated equally during plane strain deformation. Thus, in Eq. (22), p^* and p^{**} interchangeably correspond to the B and C crystallographic slip planes. $\dot{\Gamma}_{p^*}/\dot{\Gamma}_{p^{**}} = 1$ and therefore dislocation walls will not form in this crystal (Section 3.1). Also, according to Section 3.3 this crystal will not shear band.

The banding calculation predicts deformation banding at a rolling reduction of 25.2%, or $\varepsilon_{\text{vM}} \approx 0.29$. As in Section 4.1, although the Chin–Wonsiewicz condition (Eq. (11)) is always satisfied, orientational stability (Section 2.4) prevents banding for $\varepsilon_{\text{vM}} < 0.29$. Unlike in Section 4.1, however, the initial orientation of the crystal remains stable until banding. Each of the four activated slip systems harden identically. The orientational instability at $\varepsilon_{\text{vM}} \approx 0.29$ is induced solely because the orientation perturbation ω becomes large enough to induce sufficiently different deformations within the bands. At the instant of banding, the optimal (Eq. (9)) misorientation vector is parallel to the TD, in agreement with experiment. The optimal volume fraction of each band is 0.5, and the normal to the interband boundary ($\boldsymbol{v}$) is optimally oriented parallel to ND, so that the interband boundary itself coincides with the rolling plane, again in agreement with experiment.

With either the mobile or immobile boundary assumption, further deformation leaves the interband boundary aligned with the rolling plane in the present calculation. Since the predictions of both assumptions coincide, the mobility or immobility of the bands cannot be determined from these considerations. The experimental observations of Lee and Duggan [4] in copper and Wert et al. [55] in aluminum, however, suggest that deformation bands are immobile. The volume fractions of the bands are therefore held fixed during the subsequent deformation (Section 3.4).

After banding, lattice orientations of the bands (indexed by (1) and (2)) evolve along $(-90, \phi^{(1)}, 45)°$ and $(90, \phi^{(2)}, -135)°$, respectively, as shown in Fig. 6. It is seen that $\phi^{(1)} = \phi^{(2)}$. The calculated band rotations agree with those measured by Heye and Sattler [34].

Fig. 7 shows the calculated evolution of the absolute slip rates $|\dot{\gamma}|$ in both coplanar slip systems (CP1: C1 and C3; and CP2: B2 and B4) in both deformation bands (DB1 and DB2). Before banding, all four slip systems considered are identically activated. A transient response occurs immediately after banding ($0.29 \leqslant \varepsilon_{\text{vM}} \leqslant 0.33$) wherein slip rates fluctuate sharply. As in Section 4.1, we attribute this to the instantaneous introduction of bands into the computer crystal, and expect that the physical crystal will initiate the band gradually and therefore exhibit a softer transient response.

Beyond the transient response regime, it is seen that in the first deformation band (DB1), slip in CP2 (B2 and

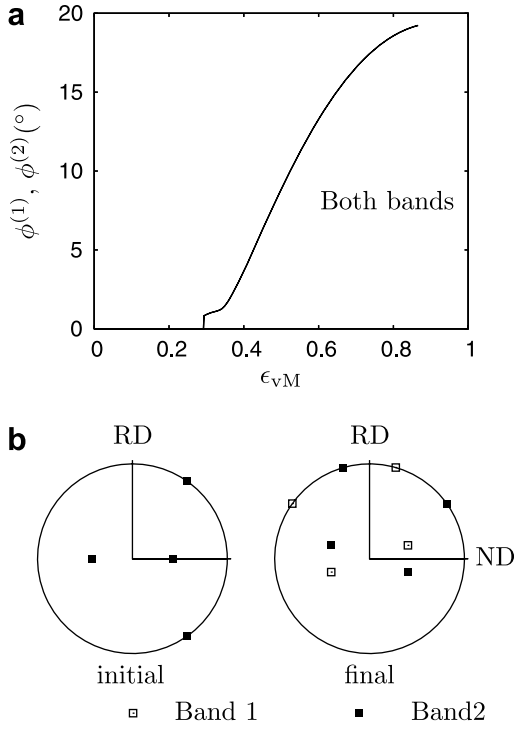

Fig. 6. (a) Evolution with deformation of the middle Bunge angle in the bands ($\phi^{(1)}$ and $\phi^{(2)}$) in an initially (0 0 1)/[1 1 0]-oriented single crystal. (b) Calculated (1 1 1) pole figures before and after 75% rolling reduction. The pole figures are oriented exactly as in Fig. 3 of Ref. [34] for easy comparison.

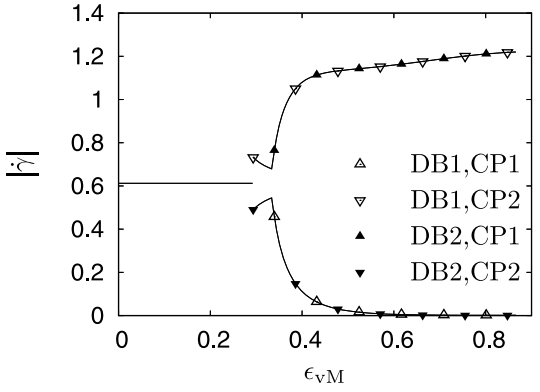

Fig. 7. Evolution of the slip activity in the two coplanar slip systems (CP1 and CP2) in both bands (DB1 and DB2) with von Mises strain in the crystal in an initially (0 0 1)/[1 1 0]-oriented single crystal.

B4) is increasingly enhanced with deformation, and that in CP1 (C1 and C3) is increasingly suppressed. The opposite occurs in deformation band 2 (DB2). Thus, slip in each band becomes increasingly confined with deformation to a pair of coplanar systems thereby reducing the latent hardening in the crystal as a whole. Unlike in Refs. [24,25] wherein the objective of reducing plastic work led to reduced latent hardening and hence to banding, the present theory deduces reduced latent hardening in the crystal through banding based on $\dot{W}^{\text{def}}$ minimization. Also, the new slip state in each band will lead to the formation of a dislocation wall in the bands parallel to the B and C crystallographic planes (Section 3.1), absent in the homogeneously deforming crystal.

The calculated velocity gradients in the bands at 75% rolling reduction are

$$[\mathbf{L}^{(1)}]_{\text{RD-TD-ND}} = \begin{pmatrix} 1.00 & 0.00 & 1.27 \\ 0.00 & 0.00 & 0.00 \\ -0.58 & 0.00 & -1.00 \end{pmatrix}, \quad \text{and}$$
$$[\mathbf{L}^{(2)}]_{\text{RD-TD-ND}} = \begin{pmatrix} 1.00 & 0.00 & -1.27 \\ 0.00 & 0.00 & 0.00 \\ 0.58 & 0.00 & -1.00 \end{pmatrix}. \tag{26}$$

The +/− pattern seen in L_{13} and L_{31} above is called the redundant shear and has been observed experimentally during rolling in a number of crystal orientations [56,57]. Lee and Duggan [58] have proposed that redundant shear is imposed by the rolls due to frictional and geometric effects. Wert [56], using an upper bound analysis that modeled rolling deformation as flow through a converging channel, found that smaller plastic work is associated with crystal deformation involving redundant shears than that with homogeneous crystal deformation. The present calculation shows that driven solely by the tendency to minimize plastic power (Eq. (19)), the velocity gradient in the bands acquires the +/− pattern in L_{13} and L_{31} even under plane strain deformation (Eq. (24)). This suggests that redundant shears are part of the intrinsic crystal response, independent of any constraints forced by the rolls or other external mechanism.

5. Conclusions

The problem of microstructural and substructural evolution in a crystal is inherently circular. Small dislocation structures determine the state of slip system hardness that govern the formation of the much larger bands. Bands in turn alter the local deformation fields and thereby affect the local hardness of the slip systems. The present theory accounts for this circularity. The crystallography of slip is taken to be the dominant influence at the scale of the smallest dislocation structures. Phenomenological information on the presence or absence of dislocation walls, and slip system hardness (Section 3) is fed from this scale to the scale of the bands, where minimization of the plastic power $\dot{W}^{\text{def}}$ (Section 2.3) and orientational instability (Section 2.4) determine the banded structure. It has been shown that the predictions of this approach agree quantitatively with the experimental observations in two rolled single crystals: one that forms shear bands (Section 4.1), and the other that forms deformation bands (Section 4.2).

Acknowledgement

The author thanks Dr. C.N. Tomé of Los Alamos National Laboratory for his valuable comments on this

manuscript. The use of Dr. Tomé's POLE software in plotting the pole figures here is also gratefully acknowledged.

References

[1] Bay B, Hansen N, Kuhlmann-Wilsdorf D. Mater Sci Eng A 1989;113:385.
[2] Kuhlmann-Wilsdorf D. Acta Mater 1999;47:1697.
[3] Hansen N, Jensen DJ. Phil Trans R Soc Lond 1999;A357:1447.
[4] Lee CS, Duggan BJ, Smallman RE. Acta Metall Mater 1993;41:2265.
[5] Liu Q, Hansen N. Proc R Soc Lond 1998;A454:2555.
[6] Kulkarni SS, Starke EAS, Kuhlmann-Wilsdorf D. Acta Mater 1998;46:5283.
[7] View point set no. 6: Shear bands, Scripta Metall 1984;18:421.
[8] Wagner P, Engler O, Lücke K. Acta Metall Mater 1995;43:3799.
[9] Hughes DA, Hansen N. Metall Trans 1993;24A:2021.
[10] Huang X, Hansen N. Scripta Mater 1997;37:1.
[11] Duggan BJ, Hatherly M, Huchinson WB, Wakefield PT. Met Sci 1978;12:343.
[12] Morii K, Mecking H, Nakayama Y. Acta Metall 1985;33:379.
[13] Nakayama Y, Morii K. Acta Metall 1987;35:1747.
[14] Hill R. J Mech Phys Solids 1962;10:1.
[15] Rudnicki JW, Rice JR. J Mech Phys Solids 1975;23:371.
[16] Asaro RJ, Rice JR. J Mech Phys Solids 1977;25:309.
[17] Asaro RJ. Acta Metall 1979;27:445.
[18] Pierce D, Asaro RJ, Needleman A. Acta Metall 1983;31:1951.
[19] Anand L, Spitzig WA. J Mech Phys Solids 1980;28:113.
[20] Anand L, Spitzig WA. Acta Metall 1982;30:553.
[21] Dillamore IL, Roberts JG, Bush AC. Met Sci 1979;13:73.
[22] Van Houtte P, Sevillano JG, Aernoudt E. Z Metallkd 1979;70:426.
[23] Lee CS, Duggan BJ. Acta Metall Mater 1993;41:2691.
[24] Ortiz M, Repetto EA. J Mech Phys Solids 1999;47:397.
[25] Ortiz M, Repetto EA, Stainier L. J Mech Phys Solids 2000;48:2077.
[26] Andrade EN, Roscoe R. Proc Phys Soc Lond 1935;49:120.
[27] Embury JD, Korbel A, Raghunathan VS, Rys J. Acta Metall 1984;32:1883.
[28] Korbel A, Embury JD, Hatherly M, Martin PL, Erbsloh HW. Acta Metall 1986;34:1999.
[29] Korbel A, Martin P. Acta Metall 1986;34:1905.
[30] Mahesh S, Tomé CN. Philos Mag 2004;84:3517.
[31] Taylor GI. J Inst Met 1938;62:307.
[32] Chin GY, Wonsiewicz BC. Trans AIME 1969;245:871.
[33] Jasienski Z, Baudin T, Piatkowski A, Penelle R. Scripta Mater 1996;35:297.
[34] Heye W, Sattler HP. Z Metallkd 1971;62:386.
[35] Asaro RJ, Needleman A. Acta Metall 1985;33:923.
[36] Canova GR, Fressengeas C, Molinari A, Kocks UF. Acta Metall 1988;38:1961.
[37] Hughes DA, Liu Q, Chrzan DC, Hansen N. Acta Mater 1997;45:105.
[38] Hill R. In: Sneddon IN, Hill R, editors. Progress in solid mechanics 2. New York (NY): Interscience; 1961. p. 247.
[39] Kelley CT. Iterative methods for optimization. Philadelphia PA: SIAM; 1999.
[40] Lee CS, Smallman RE, Duggan BJ. Scripta Metall Mater 1995;33:727.
[41] Raabe D, Zhao Z, Park SJ, Roters F. Acta Mater 2002;50:421.
[42] Cuitiño AM, Ortiz M. Modeling Simul Mater Sci Eng 1992;1:225.
[43] Franciosi P, Zaoui A. Acta Metall 1982;30:1627.
[44] Franciosi P, Zaoui A. Acta Metall 1982;30:2151.
[45] Huang X. Scripta Mater 1998;38:1697.
[46] Jackson PJ. Mater Sci Eng 1983;57:37.
[47] Kawasaki Y. In: Oikawa K et al., editors. Strength of materials. Japan Institute of Metals; 1990. p. 187.
[48] Kawasaki Y. Jpn J Appl Phys 1979;18:1429.
[49] Kawasaki Y, Takeuchi T. Scripta Metall 1980;14:183.
[50] Lee CS, Duggan BJ. Acta Metall Mater 1994;42:857.
[51] Driver JH, Jensen DJ, Hansen N. Acta Metall Mater 1994;42:3105.
[52] Godfrey A, Jensen DJ, Hansen N. Acta Metall Mater 1998;46:835.
[53] Franciosi P, Berveiller M, Zaoui A. Acta Metall 1980;28:273.
[54] Franciosi P. In: McQueen HJ et al., editors. Strength of metals and alloys 7. Oxford: Pergamon; 1986. p. 281.
[55] Wert JA, Kashihara K, Okada T, Huang X, Inoko F. Philos Mag 2005;85:1989.
[56] Wert JA. Acta Mater 2002;50:3125.
[57] Wert JA, Liu Q, Hansen N. Acta Mater 1997;45:2565.
[58] Lee CS, Duggan BJ. Metall Trans 1991;22A:2637.